Photonic crystal chips for optical communications and quantum information processing

Dirk Englund[a], Ilya Fushman[a], Andrei Faraon[a], Bryan Ellis[b] & Jelena Vučković[b]

[a] Applied Physics Department, Stanford University, Stanford CA 94305;
[b] Electrical Engineering Department, Stanford University, Stanford CA 94305

ABSTRACT

We discuss recent our recent progress on functional photonic crystals devices and circuits for classical and quantum information processing. For classical applications, we have demonstrated a room-temperature-operated, low threshold, nanocavity laser with pulse width in the picosecond regime; and an all-optical switch controlled with 60 fJ pulses that shows switching time on the order of tens of picoseconds. For quantum information processing, we discuss the promise of quantum networks on multifunctional photonic crystals chips. We also discuss a new coherent probing technique of quantum dots coupled to photonic crystal nanocavities and demonstrate amplitude and phase nonlinearities realized with control beams at the single photon level.

Keywords: quantum information, single photon source, coherent control, giant optical nonlinearity, photonic crystal, quantum dot, ultrafast laser, modulator

1. CLASSICAL INFORMATION PROCESSING WITH PHOTONIC CRYSTALS

Photonic crystals enable small-volume, high-Q cavities that enhance the spontaneous emission rate and spontaneous emission coupling efficiency β of embedded emitters. These effects can decrease turn-on time and lasing threshold.[1] Above threshold, higher pump powers lead to faster decay times due to increased stimulated emission rates. Small mode volume PC cavities can be used to achieve large photon densities and speed up this process. Compared to other types of lasers such as VCSELs, PC lasers have lower driving power, increased relaxation oscillation frequency, and potentially faster electrical modulation speed due to lower device capacitance and resistance.

Two considerations are weighed in designing fast photonic crystal lasers: the Q value must be relatively large to achieve SE Purcell enhancement and hence high SE coupling efficiency; at the same time, the cavity ring-down time $\tau_c = Q/\omega$ sets a limit on the response time of the cavity ($\omega = 2\pi/\lambda$ is the resonant frequency). We choose $Q \approx 2 \cdot 10^3$, corresponding to $\tau = 1$ ps. This value of Q is easily achieved with the the single-defect cavity shown in Fig.1(c), defined in a square photonic crystal lattice. The quadrupole mode whose field pattern is shown in the inset, has a $Q \sim 2000$ as predicted by Finite Difference Time Domain (FDTD) simulations.[2]

The single-defect PC laser has the disadvantage that output power is insufficient for most practical applications. A coupled cavity array can overcome this power limitation.[2] The coupled photonic crystal structure achieves very low group velocity in any photonic crystal direction. The 2D coupled cavity array enables even higher output powers while preserving low lasing thresholds. Similarly, coupled x- and y-dipoles modes can also be formed, as shown in Fig.1(a). Though coupled arrays of small numbers of VCSELs were previously investigated,[3,4] coupling between individual lasers is difficult and requires a rather complicated fabrication procedure. Photonic crystal nanocavity arrays allow precise control of both the uniformity and the coupling very precisely.[2] The coupled cavity array and its quadrupole field pattern are shown in Fig.1(a,b). In both modes, the in-plane electric field components E_x and E_y, as well as out-of-plane B_z, are maximized in the center of the slab. This is commonly called the transverse electric (TE)-like mode.

For QD lasers, we used higher Purcell factors with a three-hole defect cavity.[5] Though theoretically limited to $Q \sim 120{,}000$, the fabricated structure shown in Fig.2 has a quality factor that is diminished to $Q \sim 3000$ because of fabrication imperfections and material loss.[6]

Further author information: (Send correspondence to D. Englund)
E-mail: englund@stanford.edu

Active Photonic Crystals II, edited by Sharon M. Weiss, Ganapathi S. Subramania, Florencio García-Santamaría
Proc. of SPIE Vol. 7031, 70310C, (2008) · 0277-786X/08/$18 · doi: 10.1117/12.796817

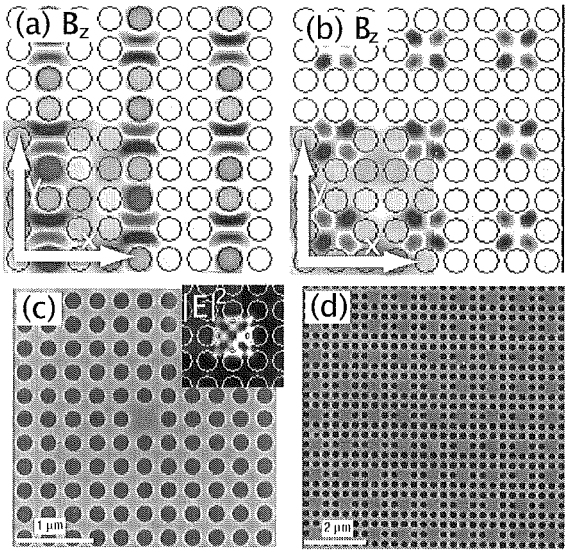

Figure 1. Square-lattice photonic crystal laser structures. (a) x-dipole-mode field pattern (out-of-plane magnetic field B_z). $y-$dipole is rotated by 90°. (b) Quadrupole mode. (c) Single-defect cavity with electric field intensity (inset). (d) Coupled cavity array structure in GaAs.

Two modulation schemes are used in telecommunications: small-signal and large-signal modulation.[7,8] In small-signal modulation, the laser is driven at a constant above-threshold pump power $L_{in,0}$ and modulated with a small signal ΔL_{in}, resulting in differential changes ΔP and ΔN_G to the steady-state photon density P_0 and lasing-level carrier densities $N_{G,0}$. In high-β lasers such as the photonic crystal device, strong cavity effects help to increase ω_R without the need to increase pump power, opening a new pathway for increasing laser modulation bandwidth.[9]

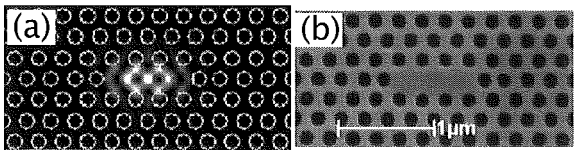

Figure 2. Three-hole defect cavity. (a) FDTD design (left, with electric field intensity) . (b) Fabricated structure in GaAs with central InGaAs QD layer.

In large-signal modulation, the rate equations predict that modulation rate is limited by the pump-level relaxation time $\tau_{E,f}$ and cavity Q. A turn-on delay arises as spontaneous emission builds the cavity field to the point when stimulated emission becomes dominant. This delay time is reduced in the high-Purcell regime through faster SE rate and higher β, as shown in Fig.3. Here the Purcell factor is calculated as

$$F = (0.5) \cdot \frac{3}{4\pi^2} \frac{Q}{V_{mode}/(\lambda/n)^3}, \tag{1}$$

where the factor 0.5 accounts for spatial averaging and is estimated from time-domain Purcell rate measurements.

2. QUANTUM WELL PHOTONIC CRYSTAL LASERS

Quantum wells provide large gain when embedded in the center of the PC cavity, where the resonant TE-like mode has the maximum electric field energy density. To reduce nonradiative (NR) surface recombination on the large QW area exposed through PC patterning, the sample was passivated in a $(NH_4)S$ solution, which

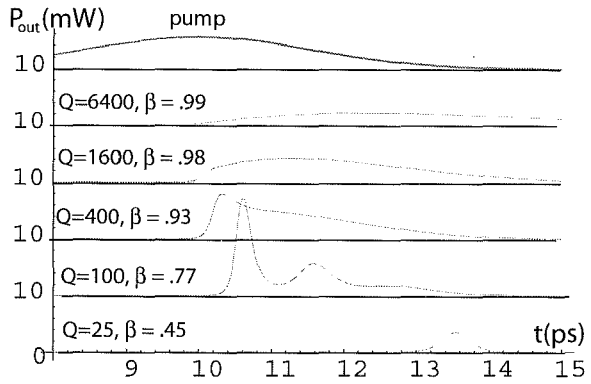

Figure 3. Calculated lasing power $P(t)\cdot(V_{mode}\hbar\omega/\tau_p)$ in response to a 3-ps pump pulse (top), for a range of Q. The turn-on delay drops with increasing Q. The excitation carrier density is $3N_{tr}$ per pulse for all plots, and pump efficiency$\eta = 1$ in this idealized model.

resulted in a 3.7-fold reduction in the lasing threshold.[10] We found that surface passivation was critical for room-temperature and continuos-wave (CW) low-temperature operation.

The structures are pumped optically with 3-ps short pulses at an 80MHz repetition rate and a wavelength centered at 750 nm using the confocal microscope as described in.[11] A 75-cm spectrometer is used for high-resolution lasing spectra, while time response is obtained using a streak camera with 3-ps resolution. For higher gain and heat dissipation, we first measured cooled structures which shifts the emission wavelength to 930 nm.[1]

The PC array laser in Fig.1(d) supports a lasing mode at $\lambda_{cav} = 950$ nm at low temperature (LT) of 10K (Fig.4(a)). Fig.4(c) shows the lasing curve for pulsed excitation (3.5 ps at 13 ns repetition), with an average threshold of 6.5 μW(measured before the objective lens). This corresponds to a large peak pump power of $\sim$ 21mW.

The threshold power is much lower under continuous pumping at low temperature, as seen in Fig.4(e). For a single cavity, threshold is even lower, near 2μW, shown in Fig.4(f). This threshold and a similarly low value recently reported with GaInAsP/InP QWs[12] are considerably lower than in previous QW lasers.[13,14]

At room temperature, threshold is higher. The lasing curve in Fig.4(d) indicates a threshold of 68 μW average power.[10] Because of faster carrier dynamics, RT operation results in faster modulation speed. This is seen in Fig.5(a) comparing RT and LT lasing response to 3.4-ps-long pump pulses (13 ns repetition).

3. QUANTUM DOT PHOTONIC CRYSTAL LASERS

We now shift to PC structures that draw gain from quantum dots instead of quantum wells. QD gain media permit lower threshold due to reduced active area (but also lower saturation power), less nonradiative surface recombination, and greater temperature stability. Their speed is set by the smaller of relaxation rate $1/\tau_{E,f}$ and relaxation oscillation rate ω_R. In ultrasmall, high-Q photonic crystal cavities, the lasing response is sped up through the Purcell effect, while large β and thus higher efficiency and lower threshold are achieved. We investigated these aspects in the 135 nm thick GaAs PC membrane shown in Fig.2(a), containing a high-density (600 μm^{-2}) of InAs QDs.

We measure a gradual onset of lasing near 1μW, as shown in Fig.6(a). From fits to the lasing curve, we estimate a SE coupling factor $\beta \sim 0.2$. Streak camera measurements of the rise time of photoluminescence from quantum dots in bulk GaAs indicate that the carrier relaxation time $\tau_{E,f} \sim 10$ ps for a wide range of pump powers. We also find that resonant pumping of higher-order confined states of the QDs (such as p-level states) does not appreciably lower $\tau_{E,f}$. Because the carrier capture time is longer than the cavity photon lifetime, it ultimately determines the maximum modulation bandwidth. This is what we observe in Fig.6(b) which shows a delay of 13.5 ps (at five times threshold) and does not drop below 12 ps for higher powers. Simulations support this observation as rise time is limited by the carrier capture time. In our cavity-QED-enhanced structure,

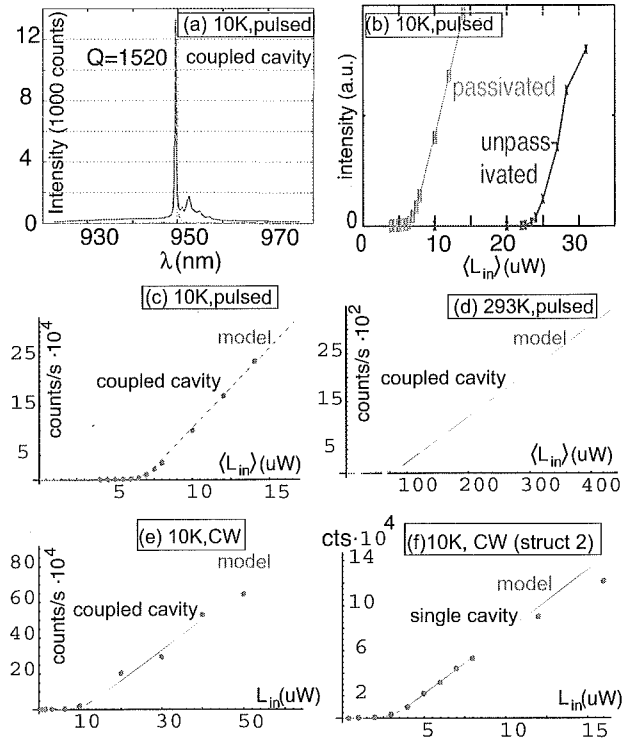

Figure 4. QW-driven PC lasing characteristics (passivated structures). (a) Coupled-cavity array spectrum below threshold and at low temperature (10K). (b) Low-temperature lasing curve shows threshold reduction after passivation. (c,d) Low- and room-temperature lasing curves with pulsed excitation (3.5-pulses at 80MHz repetition, passivated structure). (e,f) Continuous excitation lasing curves for coupled and single cavity. Horizontal axes show average pump power. Fits by a rate equations model.[10]

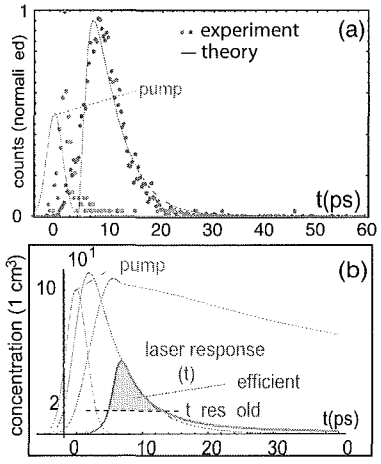

Figure 5. Laser time response. (a) Experimental data shows response nearly following the excitation pulse at room temperature; data at both temperatures are acquired at 2× lasing threshold. (b) Illustration of pump inefficiency in pulsed operation. Pump energy is efficiently channeled into the cavity mode only during lasing (shaded area under $P(t)$ curve, amplified here 5× for visibility); much of the remaining pump energy is wasted to SE and NR losses.

the relaxation-time limit is rapidly reached in the high-β case. In contrast, in non-PC quantum dot lasers not employing strong cavity effects, far higher pump power is needed to reach this limit.

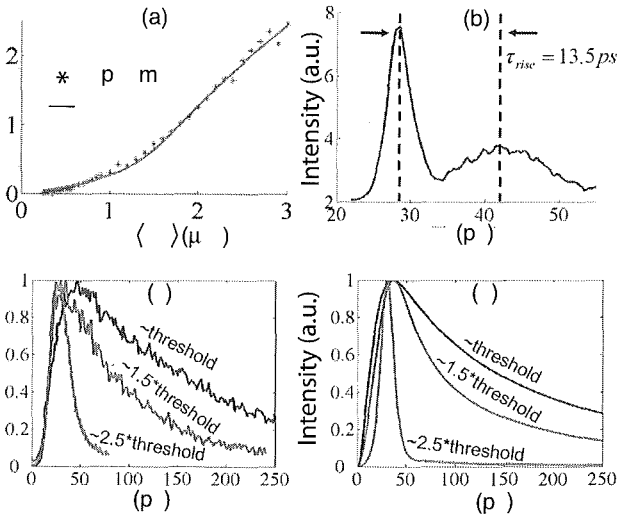

Figure 6. GaAs PC laser with InAs QD gain. (a) Measured lasing curve and fit by a rate equations model. (b) The measured turn-on delay between pump (first peak) and laser response (second peak) is limited by carrier relaxation. (c) Measured large-signal modulation speed increases with pump power. (d) Corresponding fit by rate equations.

The optically driven photonic crystal lasers described above show unprecedented speed and very low threshold. To be practical, PC lasers will need to be pumped electrically. Many groups are currently pursuing electrical pumping; one electrically driven device has already been demonstrated recently.[15] For high-speed electrical modulation, the challenge is to keep RC time constants small, where C and R are the capacitance and resistance of the laser. It appears that very fast electrical pumping of nanocavity lasers is possible, as a recent experiment achieved time constants below 10 ps using micron-scale contacts with sub-fF capacitance.[16] If fast electrical pumping can be achieved, then PC crystal lasers may well fill a growing need for integrated, ultrafast optical communication.

4. ULTRAFAST CARRIER INDUCED SWITCHING IN PHOTONIC CRYSTAL CAVITIES

The photonic crystal cavity is not only suited for emitting light, but carriers induced inside the cavity can also switch a light beam coupled through the cavity. The induced carriers temporarily change the material's refractive index, which results in a shift the cavity resonance. Such nonlinear optical switching in photonic networks is a promising approach for ultrafast low-power optical data processing and storage. In addition, it might find applications in optical data processing which will be essential for optics-based quantum information processing systems. We observed direct, ultrafast 20 GHz nonlinear optical tuning of photonic crystal PC cavities containing quantum dots QDs.[17] Switching via free-carrier generation is limited by the lifetime of free carriers and depends strongly on the material system and geometry of the device. In our case, the large surface area and small mode volume of the PC reduce the lifetime of free carriers in GaAs.

The experimental data obtained from an L3 cavity are shown in Fig.7. We used moderate energy pulses 120 fJ to shift the cavity by one-half linewidth. Stronger excitation results in higher shifts as indicated by an extremely asymmetric spectrum shown on the inset in (d) of Fig. 3, where 1.4 pJ were used. However, prolonged excitation at this power leads to a sharp reduction in Q over time.

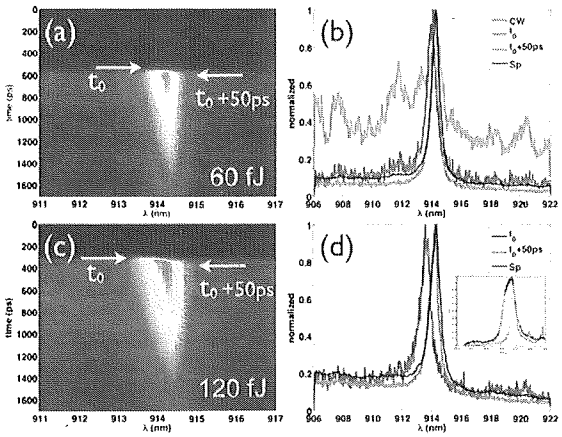

Figure 7. Experimental result of free-carrier cavity tuning. (a,b) Wavelength vs. time plots of the cavity, while the cavity is pumped. (c,d) Normalized spectra of the cavity at different time points from the data (a,b) . In (a), the cavity is always illuminated by a light source and pulsed with a 3 ps Ti:sapphire pulse. Panel (b) shows the normalized cavity spectrum at the peak of the FC distribution t=0 and 50 ps later. We verify that the cavity tunes at the arrival at the pulse by combining the pulsed excitation with a weak cw above-band pump. The emission due to the cw source is always present, and this very weak emission is reproduced in panel (b) as the broad background with a peak at the cold cavity resonace in (b).

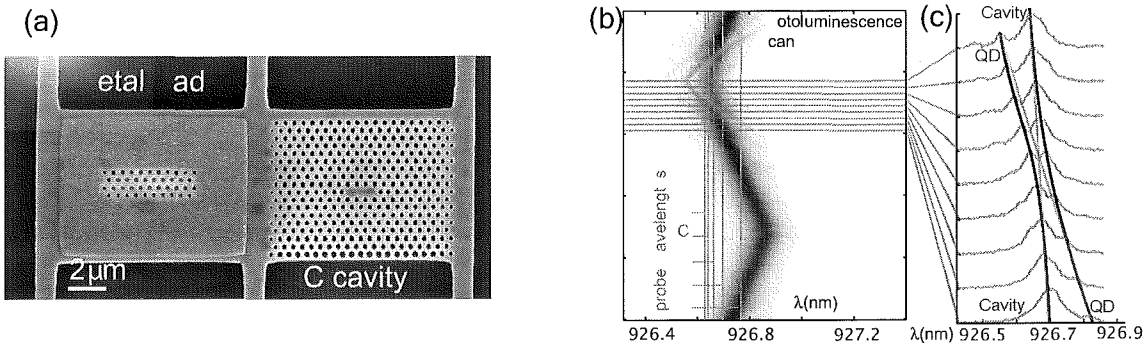

Figure 8. (a) Photonic crystal structure containing cavity and laser heating pad. (b) The spectrum of strongly coupled QD/cavity system tuned through resonance by tuning the temperature.[29] (c) Cavity/QD anticrossing. The red lines show the QD/cavity tuning if the two were uncoupled.

5. QUANTUM INFORMATION PROCESSING WITH QUANTUM DOTS IN PHOTONIC CRYSTALS

Several proposals for scalable quantum information networks and quantum computation rely on direct probing of the cavity-quantum dot coupling by means of resonant light scattering from strongly or weakly coupled dots.[18–23] Such experiments were performed in atomic systems[24–26] and superconducting circuit QED systems.[27] In 2007, we showed that the coupling between a QD and a cavity can also be probed in solid-state systems. The quantum dot (QD) strongly modifies the cavity transmission and reflection spectra as predicted[22] (this result was simultaneously reported by Srinivasan and Painter for a QD strongly coupled to a microdisk resonator[28]). When the QD is coupled to the cavity, a weak laser beam that is resonant with its transition is prohibited from coupling to the cavity. As the average probe photon number approaches unity inside the cavity, we observe a giant optical nonlinearity as the QD saturates. This technique, which we call Coherent Optical Dipole Access in a Cavity (CODAC), represents a first major step toward quantum devices based on coherent light scattering and large optical nonlinearities from QDs in photonic crystal cavities.

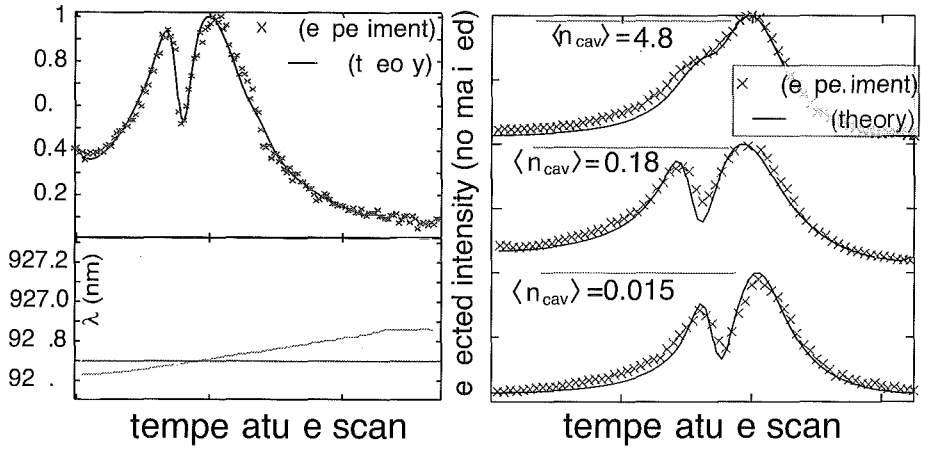

Figure 9. Resonant probing of QD/cavity system. (a) The cavity and quantum dot are scanned across the fixed probe by temperature tuning. The reflected intensity drops when the QD becomes resonant with the probe beam. (b) The QD is saturated at extremely low power, representing a large optical nonlinearity. $\langle n_{cav} \rangle$ denotes the average photon number in the cavity.

6. COHERENT ACCESS OF QUANTUM DOT - CAVITY SYSTEM

We use an L3 photonic crystal cavity[5] resonant at wavelength $\lambda_{cav} \sim 926$ nm and having quality factor $Q = 1.0 \cdot 10^4$. The structure, shown in Fig.8(a), also contains a metal pad which is used to heat the photonic crystal with an additional laser beam.[29] The cavity is strongly coupled to a QD, with a polariton splitting of 0.05nm. This splitting is seen in the (incoherent) photoluminescence (PL) measurements in Fig.8(b), where the QD is tuned through the cavity by changing the structure's temperature. Then we probed the system coherently, by reflecting a near-resonant laser beam from the cavity. The setup and measurements are given in Ref.[30] Briefly, the signal reflected by the cavity is monitored in cross-polarization with respect to the input beam to reduce background.[31] Then reflectivity is measured by temperature-tuning the cavity/QD resonances through the reflected narrow-linewidth probe laser beam. The probe's incident power is in the weak excitation limit corresponding to fewer than one photon inside the cavity per cavity lifetime (3nW measured before the objective lens), as required for probing the Vacuum Rabi splitting. As the single QD sweeps across the cavity, it coherently scatters the probe laser to interfere with the cavity signal. Instead of observing a Lorentzian-shaped cavity spectrum, a drop in the reflected signal is observed at the QD wavelength with a linewidth of g^2/κ, as expected.[22]

Earlier probing of the strongly coupled cavity/quantum dot system was done by photoluminescence.[29,32–35] Since excitons spontaneously recombine to produce the signal in these measurements, that technique represents an incoherent probing of the system. By contrast, the CODAC method described here represents a direct, coherent optical pathway to probe the system. The coherence results in the reflectivity dip: the quantum dot scatters photons π out of phase with the cavity field, which results in this case in a destructive interference.

We find good agreement between the measured reflectivity and theory,[30] using the above-mentioned cavity/QD parameters and the tracked QD and cavity wavelengths shown in the bottom of Fig. 9(a). The QD-induced feature does not reach zero because of fluctuations in the heating power (and hence QD resonance), and because of 'blinking' of the QD exciton, probably by random charging. When these are taken into account in our fit by convolving it with a Gaussian filter (FWHM=0.005 nm), the theoretical model matches the data (black fits). Another reason why the dip does not reach closer to zero, as predicted by theory, is that the dot randomly jumps between different states which can be resonant or off-resonant from the cavity. The resonant state produces a dip while the off-resonant state does not. As a consequence, the dip height is averaged between the occupation probabilities. This 'blinking' was less significant than thermal jitter in this QD/cavity, but we have observed that it can play a big role in other systems. The reason for blinking is probably a combination of random charging[36] and phonon-mediated jitter.

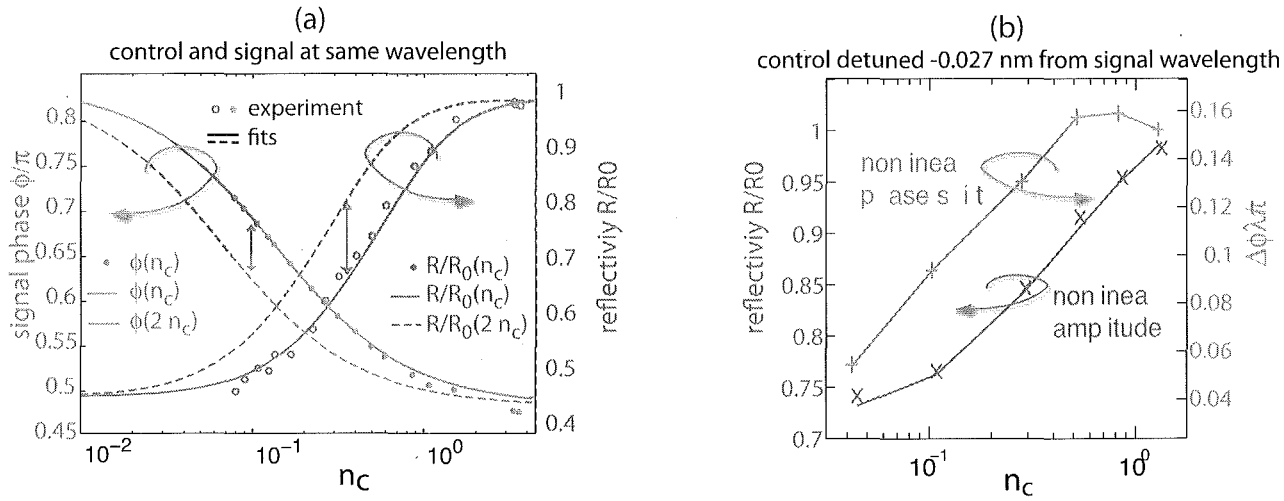

Figure 10. Saturation of the QD-induced interference and its corresponding phase. (a) The dot was detuned from the cavity by $g/3.5$; the control and probe beams are identical here. The measured saturation agrees with theory (solid line). The dashed curves show the expected phase and intensity when the control intensity is doubled. The nonlinear phase shift $\phi_r(n_c) - \phi_r(2n_c)$ is maximized at n_c=0.1, indicated by the arrow. (b) Nonlinear response to control photon number n_c when the signal beam is 0.009 nm ($\approx$ g/3) from the dot resonance (vertical lines in a,b).

7. GIANT OPTICAL NONLINEARITY

In Fig. 9(b), we show that the reflectivity of the cavity changes as the probe beam reaches $\sim$ 1 intracavity photon. P_{in} is increased from the low-excitation limit at 5 nW before the objective (corresponding to average cavity photon number $\langle n_{cav}\rangle \approx 0.003$ in a cavity without QD) to the high-excitation regime with $P_{in} \approx 12\mu$W (corresponding $\langle n_{cav}\rangle \approx 7.3$). Here, $\langle n_{cav}\rangle$ is estimated as $\eta P_{in}/2\kappa\hbar\omega_c$, where $\eta \approx 1.8\%$ is the coupling efficiency into the cavity at this wavelength. We modeled the saturation behavior by a steady-state solution of the quantum master equation following Ref. 37 using independently measured system parameters.[30] We see very good agreement over three orders of magnitude of the pump power.[30]

Since the QD-induced feature is an interference between the cavity field and the dot-scattered field, we can use its rapid saturation to change the phase of a signal beam with the field of a control beam. We measure the phase of cavity-reflected photons by interfering them with a reference beam of known intensity and phase.[38,39]

When the control and signal are at the same wavelength, the nonlinear interaction between them (Fig. 10 (a)) arises from the saturation of the QD in the presence of cavity coupled photons.[30] We observe a phase change of 0.24π (43°) when the control photon number is increased from n_c=0.08 to 3. R/R_0 increases from 0.5 to 1.0 at saturation. In these measurements, the wavelength is red-detuned by $\sim$ 0.014 nm ($g/3.5$) from the anti-crossing point (see Ref.[38]).

It may be easier to separate control and signal beams in wavelength. In that case, the signal and control beams would clearly no longer be interchangeable. But detuned beams would be perfectly suited for applications such as quantum quantum nondemolition (QND) detection, where the control beam accumulates a phase in the presence of the signal beam, or all-optical control, where a control beam switches the transmission of the cavity to the signal beam. For this measurement, we consider another dot that is also strongly coupled with a vacuum Rabi frequency $g/2\pi$ = 8GHz. We detuned the control beam by $\Delta\lambda = -0.027$ nm ($\simeq g$) from the signal beam. With a constant signal intracavity number $n_s \approx 0.2$, we then varied the control photon number n_c. The photon-photon interaction is mediated primarily by the QD saturation through the control beam, though some detuning occurs by the AC Stark effect, which can create large phase shifts.[40] In Fig. 10(b), we plot the phase and intensity of the signal beam when it is red-detuning by $0.4g$ from the cavity, which in turn is resonant with the QD. Here the phase is plotted with respect to the phase when the control beam is off, $\Delta\phi_r = \phi_r - \phi_r(n_c = 0) \equiv \phi_r - \phi_{r,0}$.

Quantum gates require a large phase change of a signal photon, conditioned on a single control photon.[41–43] Furthermore, they require that both signal and control photons have the same wavelength and duration. We

measured the differential phase change by the difference between the phase evaluated at n_c and $2n_c$ (Fig. 10(a)). This gave a maximum differential phase shift of 0.07π (12°) at n_c =0.1 and maximum amplitude change of 15% at n_c=0.43. Theoretically we estimate a maximum of $\simeq 0.15\pi$ (27°) for phase and 20% amplitude modulation with our system parameters, when the quantum dot is tuned on resonance with the cavity. In applications where a large phase change is required, it may be preferable to detune the quantum dot from the cavity. Then the phase change can reach 0.4π at a moderate QD-cavity detuning of $3g$, as detailed in Ref.[39]

A controlled phase gate requires a π phase shift.[43,44] Relying on the saturation of the dot, this would require repeated interactions, possibly by cascading several QD/cavity systems in series. In this case, the coupling losses would grow exponentially. A more efficient, on-chip integrated architecture,[45] promises to improve efficiencies. A second, though smaller, source of coherence loss is QD spontaneous emission. It is fortuitous that the spontaneous emission into non-cavity modes is suppressed by the PC bandgap.[46]

The direct photonic access demonstrated here enables a giant nonlinear optical response of the QD/cavity system, occurring at the single photon level.[30] This nonlinearity allows conditional phase and amplitude changes of a signal photon via a control photon.[38] From simulations, we expect that when the QD is detuned from the cavity, a single control photon can change the phase of a signal photon by as much as 0.4π.[39] Alternatively, the signal photon's phase may be changed by as much as π by AC-stark shift of a control photon. A controlled $\pi-$ gate would enable a full set of quantum logic gates.[44] From measurements of the second-order coherence function, we also demonstrated that the cavity/QD system provides a photon-photon interaction which results in either photon blockade or photon-induced tunneling.[47] These results suggest that the QD/cavity system is very promising for quantum and classical information processing. Currently, the coupling efficiencies into and out of the cavity are still low – on the order of 2-5%. By adopting an on-chip approach and exploring better off-chip couplers, we hope to bring this efficiency near unity and thus enable efficient, controlled interactions between single photons.

REFERENCES

[1] Altug, H., Englund, D., and Vučković, J., "Ultrafast photonic crystal nanocavity laser," *Nature Physics* **2**, 484–488 (2006).

[2] Altug, H. and Vuckovic, J., "Experimental demonstration of the slow group velocity of light in two-dimensional coupled photonic crystal microcavity arrays," *Appl. Phys. Lett.* **86**(11), 111102 (2005).

[3] Deppe, D. G., van der Ziel, J. P., Chand, N., Zydzik, G. J., and Chu, S. N. G., "Phase-coupled two-dimensional $Al_xGa_{1-x}As$-GaAs vertical-cavity surface-emitting laser array," *Appl. Phys. Lett.* **56**(21), 2089–2091 (1990).

[4] James J. Raftery, J., Danner, A. J., Lee, J. C., and Choquette, K. D., "Coherent coupling of two-dimensional arrays of defect cavities in photonic crystal vertical cavity surface-emitting lasers," *Appl. Phys. Lett.* **86**(20), 201104 (2005).

[5] Akahane, Y., Asano, T., Song, B.-S., and Noda, S., "High-Q photonic nanocavity in a two-dimensional photonic crystal," *Nature* **425**, 944–947 (Oct. 2003).

[6] Englund, D., Fushman, I., and Vučković, J., "General Recipe for Designing Photonic Crystal Cavities," *Opt. Express* **12**, 5961–75 (Aug. 2005).

[7] Coldren, L. A. and Corzine, S. W., [*Diode Lasers and Photonic Integrated Circuits*], Wiley, New York (1995).

[8] Chang, C. H., Chrostowski, L., and Chang-Hasnain, C. J., "Injection locking of VCSELs," *J. Sel. Top. Quantum Electron.* **9**, 1386–1393 (2003).

[9] Bjork, G. and Yamamoto, Y., "Analysis of semiconductor microcavity lasers using rate equations," *IEEE Journal of Quantum Electonics* **27**, 2386–96 (Nov. 1991).

[10] Englund, D., Altug, H., and Vučković, J., "Low-Threshold Surface-Passivated Photonic Crystal Nanocavity Laser," *Appl. Phys. Lett.* **91**, 071124 (July 2007).

[11] Englund, D., Altug, H., Fushman, I., and Vučković, J., "Efficient Terahertz Room-Temperature Photonic Crystal Nanocavity Laser," *Appl. Phys. Lett.* **91**, 071126 (July 2007).

[12] Nozaki, K., Kita, S., and Baba, T., "Room temperature continuous wave operation and controlled spontaneous emission in ultrasmall photonic crystal nanolaser," *Opt. Express* **15**(12), 7506–7514 (2007).

[13] Nomura, M., Iwamoto, S., Nishioka, M., Ishida, S., and Arakawa, Y., "Highly efficient optical pumping of photonic crystal nanocavity lasers using cavity resonant excitation," *Appl. Phys. Lett.* **89**(161111) (2006).

[14] Shih, M. H., Kuang, W., Mock, A., Bagheri, M., Hwang, E. H., O'Brien, J., and Dapkus, P., "High-quality-factor photonic crystal heterostructure laser," *Appl. Phys. Lett.* **89**(101104) (2006).

[15] Park, H., Kim, S., Kwon, S., Ju, Y., Yang, J., Baek, J., Kim, S., and Lee, Y., "Electrically driven single-cell photonic crystal laser," *Science* **305**, p.1444–7 (2004).

[16] Schmidt, R., Scholz, U., Vitzethum, M., Fix, R., Metzner, C., Kailuweit, P., Reuter, D., Wieck, A., Hübner, M. C., Stufler, S., Zrenner, A., Malzer, S., and Döhler, G. H., "Fabrication of genuine single-quantum-dot light-emitting diodes," *Appl. Phys. Lett.* **88**(12), 121115 (2006).

[17] Fushman, I., Waks, E., Englund, D., Stoltz, N., Petroff, P., and Vučković, J., "Ultrafast nonlinear optical tuning of photonic crystal cavities," *Appl. Phys. Lett.* **90**(9), 091118 (2007).

[18] Cirac, J. I., Zoller, P., Kimble, H. J., and Mabuchi, H., "Quantum State Transfer and Entanglement Distribution among Distant Nodes in a Quantum Network," *Phys. Rev. Lett.* **78**, 3221–24 (Apr. 1997).

[19] Imamoğlu, A., Awschalom, D. D., Burkard, G., DiVincenzo, D. P., Loss, D., Sherwin, M., and Small, A., "Quantum Information Processing Using Quantum Dot Spins and Cavity QED," *Phys. Rev. Lett.* **83**, 4204–4207 (Nov. 1999).

[20] Duan, L.-M. and Kimble, H. J., "Scalable photonic quantum computation through cavity-assisted interactions," *Phys. Rev. Lett.* **92**(12), 127902 (2004).

[21] Childress, L., Taylor, J. M., Sorensen, A. S., , and Lukin, M. D., "Fault-tolerant quantum repeaters with minimal physical resources and implementations based on single-photon emitters," *Phys. Rev. A* **72**, 052330 (2005).

[22] Waks, E. and Vučković, J., "Dipole induced transparency in drop-filter cavity-waveguide systems," *Phys. Rev. Lett.* **96** (April 2006).

[23] Ladd, T. D., van Loock, P., Nemoto, K., Munro, W. J., and Y.Yamamoto, "Hybrid quantum repeater based on dispersive CQED interactions between matter qubits and bright coherent light," *New Journal of Physics* **8**, 184 (2006).

[24] Birnbaum, K. M., Boca, A., Miller, R., Boozer, A. D., Northup, T. E., and Kimble, H. J., "Photon blockade in an optical cavity with one trapped atom," *Nature* **436**, 87–90 (2005).

[25] Rauschenbeutel, A., Nogues, G., Osnaghi, S., Bertet, P., Brune, M., Raimond, J. M., and Haroche, S., "Coherent Operation of a Tunable Quantum Phase Gate in Cavity QED," *Phys. Rev. Lett.* **83**, 5166–5169 (1999).

[26] Nogues, G., Rauschenbeutel, A., Osnaghi, S., Brune, M., Raimond, J. M., and Haroche, S., "Seeing a single photon without destroying it," *Nature* **400**, 239–242 (1999).

[27] Schuster, D. I., Houck, A. A., Schreier, J. A., Wallraff, A., Gambetta, J. M., Blais, A., Frunzio, L., Majer, J., Johnson, B., Devoret, M. H., Girvin, S. M., and Schoelkopf, R. J., "Resolving photon number states in a superconducting circuit," *Nature* **445**, 515–18 (Feb 2007).

[28] Srinivasan, K. and Painter, O., "Linear and nonlinear optical spectroscopy of a strongly coupled microdisk-quantum dot system," *Nature* **450**, 862–865 (Dec. 2007).

[29] Faraon, A., Englund, D., Fushman, I., Stoltz, N., Petroff, P., and Vučković, J., "Local quantum dot tuning on photonic crystal chips," *Appl. Phys. Lett.* **90** (May 2007).

[30] Englund, D., Faraon, A., Fushman, I., Stoltz, N., Petroff, P., and Vučković, J., "Controlling cavity reflectivity with a single quantum dot," *Nature* **450**(6), 857–61 (2007).

[31] Altug, H. and Vuckovic, J., "Polarization control and sensing with two-dimensional coupled photonic crystal microcavity arrays," *Opt. Lett.* **30**(9), 982–984 (2005).

[32] Yoshie, T., Scherer, A., Hendrickson, J., Khitrova, G., Gibbs, H. M., Rupper, G., Ell, C., Shchekin, O. B., and Deppe, D. G., "Vacuum Rabi splitting with a single quantum dot in a photonic crystal nanocavity," *Nature* **432**, 200–203 (Nov. 2004).

[33] Hennessy, K., Badolato, A., Winger, M., Gerace, D., Atature, M., Gulde, S., Falt, S., Hu, E. L., and Imamoglu, A., "Quantum nature of a strongly coupled single quantum dot-cavity system," *Nature* **445**, 896–899 (2007).

[34] Peter, E., Senellart, P., Martrou, D., Lemaître, A., Hours, J., Gérard, J. M., and Bloch, J., "Exciton-photon strong-coupling regime for a single quantum dot embedded in a microcavity," *Physical Review Letters* **95**(6), 067401 (2005).

[35] Reithmaier, J. P., Sek, G., Loffler, A., Hofmann, C., Kuhn, S., Reitzenstein, S., Keldysh, L. V., Kulakovskii, V. D., Reinecke, T. L., and Forchel, A., "Strong coupling in a single quantum dotsemiconductor microcavity system," *Nature* **432**, 197–200 (2004).

[36] Santori, C., Fattal, D., Vučković, J., Solomon, G. S., Waks, E., and Yamamoto, Y., "Submicrosecond correlations in photoluminescence from inas quantum dots," *Phys. Rev. B* **69**, 205324 (May 2004).

[37] Tan, S. M., "A computational toolbox for quantum and atomic physics," *J. Opt. B: Quantum Semiclass. Opt.* **1**, 424–432 (1999).

[38] Fushman, I., Englund, D., Faraon, A., Stoltz, N., Petroff, P., and Vuckovic, J., "Controlled Phase Shifts with a Single Quantum Dot," *Science* **320**(5877), 769–772 (2008).

[39] Englund, D., *Photonic Crystals for Quantum and Classical Information Processing*, PhD thesis, Stanford University (July 2008).

[40] Waks, E. and Vuckovic, J., "Dispersive properties and large kerr nonlinearities using dipole-induced transparency in a single-sided cavity," *Physical Review A (Atomic, Molecular, and Optical Physics)* **73**(4), 041803 (2006).

[41] Chuang, I. L. and Yamamoto, Y., "Simple quantum computer," *Phys. Rev. A* **52**, 3489–3496 (Nov 1995).

[42] Nemoto, K. and Munro, W. J., "Nearly deterministic linear optical controlled-not gate," *Phys. Rev. Lett.* **93**, 250502 (Dec 2004).

[43] Turchette, Q., Hood, C., Lange, W., Mabuchi, H., and Kimble, H. J., "Measurement of conditional phase shifts for quantum logic," *Phys. Rev. Lett.* **75**, 4710–4713 (1995).

[44] Nielsen, M. A. and Chuang, I. L., [*Quantum Computation and Quantum Information*], Cambridge Univ. Press, Cambridge (2000).

[45] Englund, D., Faraon, A., Zhang, B., Yamamoto, Y., and Vuckovic, J., "Generation and transfer of single photons on a photonic crystal chip," *Opt. Express* **15**, 5550–8 (Apr. 2007).

[46] Englund, D., Fattal, D., Waks, E., Solomon, G., Zhang, B., Nakaoka, T., Arakawa, Y., Yamamoto, Y., and Vučković, J., "Controlling the Spontaneous Emission Rate of Single Quantum Dots in a Two-Dimensional Photonic Crystal," *Phys. Rev. Lett.* **95**, 013904 (July 2005).

[47] Faraon, A., Fushman, I., Englund, D., Stoltz, N., Petroff, P., and Vuckovic, J., "Coherent generation of nonclassical light on a chip via photon-induced tunneling and blockade," *quant-ph/0804.2740v1* (2008).